Single-Shot Readout of a Nuclear Spin in Silicon Carbide

Xiao-Yi Lai,[1,2,3,*] Ren-Zhou Fang,[1,2,3,*] Tao Li,[1,2,3] Ren-Zhu Su,[1,2,3] Jia Huang,[4] Hao Li,[4] Li-Xing You,[4]
Xiao-Hui Bao,[1,2,3] and Jian-Wei Pan[1,2,3]

[1]*Hefei National Research Center for Physical Sciences at the Microscale and School of Physical Sciences,*
University of Science and Technology of China, Hefei 230026, China
[2]*CAS Center for Excellence in Quantum Information and Quantum Physics,*
University of Science and Technology of China, Hefei 230026, China
[3]*Hefei National Laboratory, University of Science and Technology of China, Hefei 230088, China*
[4]*Shanghai Key Laboratory of Superconductor Integrated Circuit Technology,*
Shanghai Institute of Microsystem and Information Technology, Chinese Academy of Sciences, Shanghai 200050, China

Solid-state qubits with a photonic interface is very promising for quantum networks. Color centers in silicon carbide have shown excellent optical and spin coherence, even when integrated with membranes and nanostructures. Additionally, nuclear spins coupled with electron spins can serve as long-lived quantum memories. Pioneering work previously has realized the initialization of a single nuclear spin and demonstrated its entanglement with an electron spin. In this Letter, we report the first realization of single-shot readout for a nuclear spin in SiC. We obtain a deterministic nuclear spin initialization and readout fidelity of 94.95% with a measurement duration of 1 ms. With a dual-step readout scheme, we obtain a readout fidelity as high as 99.03% within 0.28 ms by sacrificing the success efficiency. Our Letter complements the experimental toolbox of harnessing both electron and nuclear spins in SiC for future quantum networks.

Solid-state color centers are promising systems to demonstrate quantum computing and quantum information processes [1]. One of the most studied solid-state systems is negatively charged nitrogen-vacancy centers in diamond, which have been used widely in quantum network and quantum sensing [2]. However, there still lacks a mature growing and nanofabrication method for diamond crystals, which is a strict obstacle for large scale quantum applications. The color centers in silicon carbide (SiC) are promising candidates [3–5] with the addition of a material advantage including wafer scaling [6] and mature fabrication [7]. Rapid developments with color centers in SiC have been shown during these years, including high fidelity spin and optical control [8,9], millisecond electron spin coherence time in isotopic purified material [10], two-photon interference [11], efficiency spin-photon interface with high coherence [12], single-shot readout by spin-charge conversion [13], and spin-photon entanglement [14]. Typically, the V2 centers in SiC have shown excellent properties, e.g., high optical coherence when temperature is up to 20 K [15] and higher quantum efficiency compared to V1 centers in SiC [16], and can maintain narrow optical linewidth even when created by ion implantation or integrated in waveguides [12], microcavities [17], and submicromembranes [18]. However, due to large gyromagnetic ratios, electron spins couple strongly with the crystal local environment, which induce the coherence time of

electron spins that are strictly limited by impurities and nuclear baths in the crystal [19].

Nuclear spins are crucial resources for quantum computation and quantum information [20]. With less coupling with the local crystal environment compared with electron spins, nuclear spins usually possess long coherence time, making them almost perfect quantum memories [21]. Nuclear spins in SiC have rapid developments, and many milestone experiments have been demonstrated, such as entanglement between electron-nuclear spin ensembles at room temperature [22], single nuclear spin initialization [23], entanglement between a single divacancy, and a strongly coupled nuclear spin [10]. However, the single-shot readout of a nuclear spin is still yet to be realized.

In this Letter, we report the first realization of single-shot readout of a nuclear spin in SiC. We choose a next-nearest-neighbor (NNN) ^{29}Si nuclear spin that is strongly coupled with a k-site silicon-vacancy (V2) center [Fig. 1(a)]. The V2 center in commercial natural abundance 4H-SiC is created by electron irradiation and postannealing, we fabricate solid immersion lens and coat Al_2O_3 film in the a side to enhance collection efficiency. The sample is placed into a 4 K cryostat, and a confocal system is established to excite V2 and collect fluorescence from V2. The objective is outside the cryostat, with NA = 0.65. The zero phonon line (ZPL) wavelength of V2 centers in 4H-SiC is 916 nm, and we collect phonon sideband (PSB)
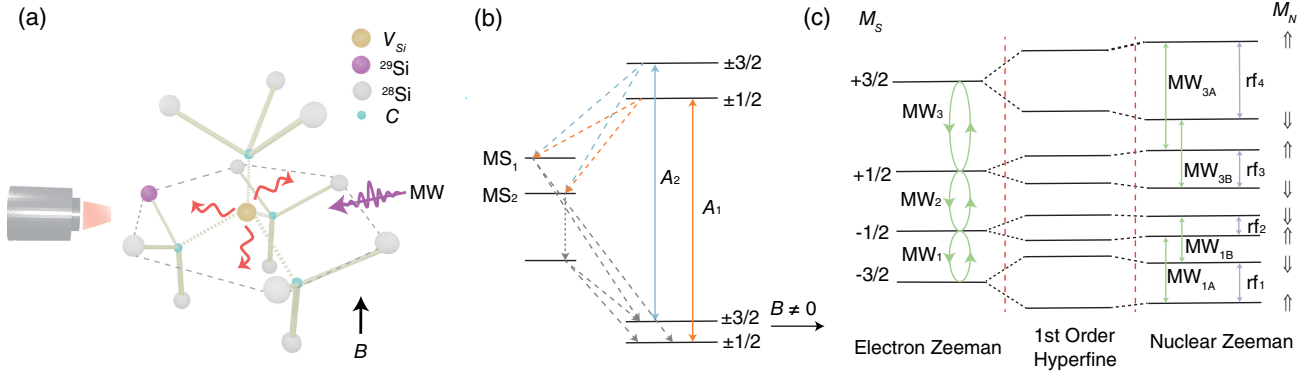
FIG. 1. Energy level of a V2 center strongly coupled with a NNN ^{29}Si nuclear spin. (a) Atomic model of the negatively charged silicon-vacancy defect in 4H-SiC. In plane NNN Si atoms are connected by dotted lines for marking. 4H-SiC c axis is parallel to the external magnetic field, and the fluorescence from the V2 center is collected perpendicular to the c axis. (b) Energy level diagram of V2 centers at zero external magnetic field. (c) Ground-state level structure of a V2 center strongly coupled with a single nuclear spin under external magnetic field. MW2 is not used in this Letter.

fluorescence above 930 nm to filter resonant excitation laser noise. The external magnetic field is 960 G, the main component of external magnetic field is provided by two permanent magnets installed on both sides of the sample stage, and the small angle misalignment compared to c axis is compensated by a permanent magnet outside the cryostat. Under this external magnetic field, the V2 center electron Zeeman splitting is much larger than electron-nuclear hyperfine splitting and the flip-flop process between electron and nuclear spins is strongly suppressed, which is the basis of our single-shot readout process. There are two types of NNN Si atoms locations: in one, the nuclear spin and V2 center are in the same plane perpendicular to the crystal c axis, and the other is out of the plane, as shown in Fig. 1(a). To further suppress the flip-flop process between V2 center and nuclear spin, we choose the NNN ^{29}Si nuclear spin in the first location [purple atom in Fig. 1(a)] to demonstrate the experiment in the following. To demonstrate nuclear spin single-shot readout, we first initialize the V2 electron spin, then the nuclear spin is initialized by applying a SWAP gate between electron and nuclear spin [24]. Finally, the single-shot readout of nuclear spin is based on 250 readout cycles; each readout cycle contains two controlled-NOT (CNOT) operations that map a specific nuclear spin state onto the electron spin [25] and an electron readout pulse that can selectively read out the electron states.

According to recent work about the intrinsic spin dynamics of V2 center, we can simply treat the energy level structure of V2 center as a six-level system [16] when the external magnetic field is zero, as shown in Fig. 1(b). We assign the transition from $|\pm1/2\rangle$ excited states to $|\pm1/2\rangle$ ground states as $A1$ transition and assign the transition from $|\pm3/2\rangle$ excited states to $|\pm3/2\rangle$ ground states as $A2$ transition. The ground-state level structure of a V2 strongly coupled with a single ^{29}Si nuclear spin under external magnetic field is shown in Fig. 1(c). In the

following, for V2 center electron spin, we denote the four states as $|+3/2\rangle$, $|+1/2\rangle$, $|-1/2\rangle$, and $|-3/2\rangle$, and for ^{29}Si nuclear spin, we denote $|+1/2\rangle$ as $|\Uparrow\rangle$ and denote $|-1/2\rangle$ as $|\Downarrow\rangle$.

The optical and spin coherence of V2 centers perform well in our system. We sweep the wavelength of a weak continuous resonant excitation laser around 916.4 nm for 20 min and collect PSB to determine the resonant frequency; the resonant frequency is very stable, as shown in Fig. 2(a). After determining the frequencies of $A1$ and $A2$ transition, we apply an 1 ns optical resonant pulse to measure the lifetime of both transitions, which are 6.45 and 10.58 ns, respectively. The lifetime of $A2$ transition is much longer than the lifetime of $A1$ transition, and this means
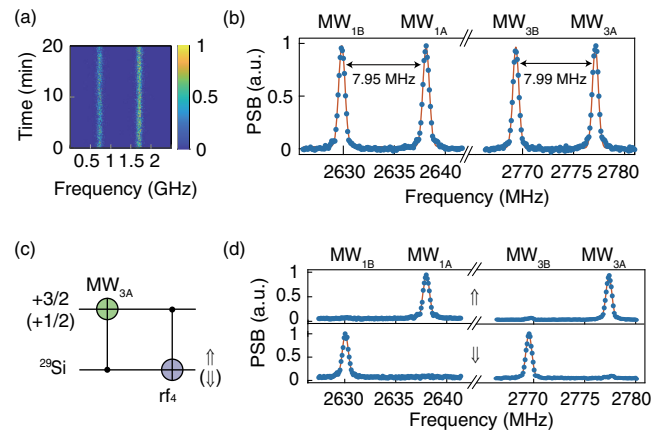

FIG. 2. Electron spin properties and nuclear spin initialization. (a) Resonant excitation scans over 20 min. (b) ODMR signal of ground states under 960 G external magnetic field; the hyperfine splitting is about 8 MHz. (c) SWAP gate between nuclear spin and V2 electron spin. The electron spin is initialized in $|+3/2\rangle$ ($|+1/2\rangle$); the nuclear spin is swapped to $\Uparrow$ ($\Downarrow$) after applying the SWAP gate. (d) ODMR signal of ground states after nuclear initialization; one of the two peaks separated by 8 MHz disappears.

higher quantum efficiency of $A2$ transition. To measure the electron optically detected magnetic resonance (ODMR) spectra, we sweep the microwave frequency with step of 0.1 MHz. As we can see in Fig. 2(b), the hyperfine splitting is about 8 MHz. We measure the fidelity of MW3A π pulse (0.37 μs) by fitting the decay of several period Rabi oscillations, and the fidelity is about $98.1 \pm 0.4\%$, which is limited by the short $T2^*$ coherence time (≈ 0.8 μs). Nuclear spin shows long coherent time in our commercial 4H-SiC crystal without isotope engineering. The $T2^*$ coherence time of 9.9 ± 1.2 ms is characterized by Ramsey sequence. The $T2^*$ coherence time of nuclear spin is 4 orders longer than the V2 electron spin, confirming that the nuclear spins are almost perfect quantum memories even in commercial SiC crystals. The nuclear spin $T1$ time is far longer than 1 s, so the influence of nuclear spin relaxation can be neglected in our single-shot readout process.

Nuclear spin initialization is an essential step for nuclear single-shot readout measurement and for nuclear-photon entanglement. We first initialize the V2 spin to $|+3/2\rangle$ ($|+1/2\rangle$) state by applying $A1$ ($A2$) laser combining with MW1A and MW1B for 60 μs with 99% fidelity. When initializing to $|+3/2\rangle$ ($|+1/2\rangle$) state, the $A1$ ($A2$) laser makes sure there is no population in $|\pm 1/2\rangle$ ($|\pm 3/2\rangle$), and the MW1A and MW1B make sure the population in $|-3/2\rangle$ ($|-1/2\rangle$) will also be rotated and pumped away. Next, we apply a SWAP gate [Fig. 2(c)] to swap the electron spin state to nuclear spin state, and the nuclear spin is initialized in $|\Uparrow\rangle$ ($|\Downarrow\rangle$). To test the fidelity of nuclear spin initialization, we measure the V2 center electron spin ODMR signal after the SWAP gate. As we can see in Fig. 2(d), one of the two peaks separated by 8 MHz disappears after the nuclear spin is initialized in $|\Uparrow\rangle$ ($|\Downarrow\rangle$). We can conclude that the fidelity of nuclear initialization is about $96 \pm 0.5\%$.

We now proceed to single-shot readout of NNN ^{29}Si nuclear spin. As depicted in Fig. 3(a), we initialize the nuclear spin in $|\Uparrow\rangle$ or $|\Downarrow\rangle$ state, and then apply 10 μs weak continuous $A2$ laser to pump the electron spin population to $|\pm 1/2\rangle$ states. Finally, we readout the nuclear spin state by repeating the readout cycles. During each cycle, we first apply two CNOT operations (MW1A and MW3A π pulse) on V2 electron spin, then apply 1.5 μs $A2$ readout laser. The CNOT gates will flip the V2 electron spin population back to the $|\pm 3/2\rangle$ state only if the nuclear spin is in the $|\Uparrow\rangle$ state, so that the V2 center can emit photons in the next readout cycle. The optical pumping fidelity of the 1.5 μs $A2$ laser reaches over 98.5% [Fig. 3(b), gray shaded area]. According to the readout sequence, the nuclear $|\Uparrow\rangle$ state will give a bright result, and the nuclear $|\Downarrow\rangle$ state will give a dark result.

Before single-shot readout, we first investigate the electron-nuclear flip-flop process during 500 readout cycles, as shown in Fig. 3(c). Ideally, if the nuclear spin is initialized in $|\Uparrow\rangle$ state [Fig. 3(c), orange], the photon
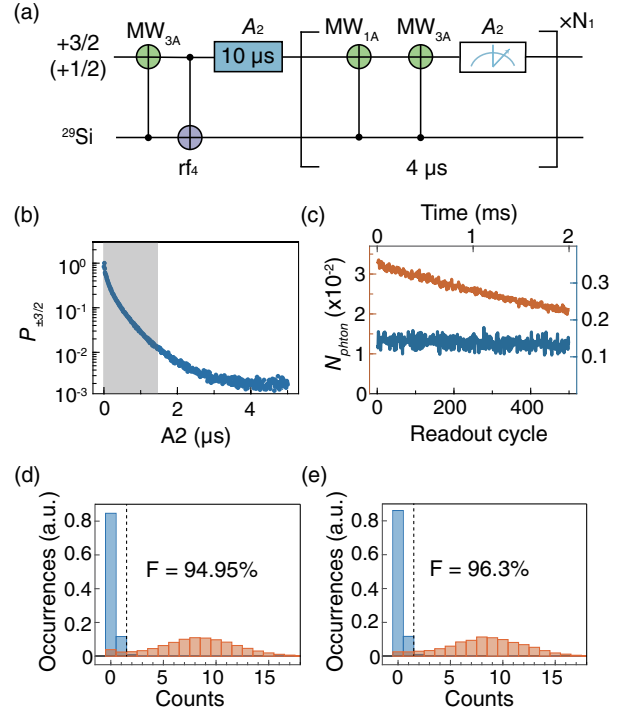

FIG. 3. Nuclear spin single-shot readout. (a) Representation of the nuclear spin single-shot readout scheme. (b) The photoluminescence signal during 5 μs $A2$ laser excitation. The optical pumping fidelity of the first 1.5 μs reaches over 98.5% (gray shaded area). (c) Photon number detected from 1.5 μs $A2$ laser during 500 readout cycles after nuclear spin initialized in $|\Uparrow\rangle$ (orange) and $|\Downarrow\rangle$ (blue). (d) Photon-count distribution for nuclear spin single-shot readout after initialized in $|\Uparrow\rangle$ (orange bar) and $|\Downarrow\rangle$ (blue bar) with $N_1 = 250$. The raw fidelity is $94.95 \pm 0.15\%$, which includes imperfection from nuclear spin initialization and readout. The average photons detected from $|\Uparrow\rangle$ ($|\Downarrow\rangle$) state is 8.14 (0.36). (e) The conditional photon-count distribution with $N_1 = 280$ shows the average single-shot readout fidelity reaching $96.3 \pm 0.16\%$.

numbers detected during each readout cycle among 500 readout cycles are almost the same, which should equal to 3.35×10^{-2}. However, the photon number decays from the first to the last cycle, meaning that there is a small possibility for each readout cycle that the nuclear spin flips from $|\Uparrow\rangle$ to $|\Downarrow\rangle$. From this result, we deduce the nuclear flipping possibility of 9.1×10^{-2} for each readout cycle.

Next, we perform a nuclear spin single-shot readout experiment, each single-shot readout process containing one nuclear spin initialization and 250 readout cycles; the total duration of each readout experiment is 1.08 ms. Before nuclear spin initialization, we check the charge state by applying 0.1 ms $A1$ and $A2$ excitation. If we detect at least two photons during 0.1 ms, we refer to it as the correct charge state. We save the latter initialization and readout results only when the charge state is correct. We count the number of photons detected in each single-shot readout process and create a histogram, as depicted in Fig. 3(d).

The nuclear spin is initialized in $|\Uparrow\rangle$ (orange bar) or $|\Downarrow\rangle$ (blue bar). We set $N = 2$ as the cutoff [the dashed line in Fig. 3(d)], corresponding to a false-negative rate $p(\Uparrow|\Downarrow) = 0.064$ and false-positive rate $p(\Downarrow|\Uparrow) = 0.037$. $p(\Uparrow|\Downarrow)$ means the nuclear state is in the $|\Uparrow\rangle$ state, but the single-shot readout result refers to the $|\Downarrow\rangle$ state, and $p(\Downarrow|\Uparrow)$ means the nuclear state is in the $|\Downarrow\rangle$ state, but single-shot readout result refers to the $|\Uparrow\rangle$ state. The overall fidelity of initialization and single-shot readout is $94.95 \pm 0.15\%$.

To exclude the infidelity from nuclear initialization, we use the first 30 readout cycles to check the initialization result. If we detect at least three photons in the first 30 readout cycles, we refer it as the $|\Uparrow\rangle$ state, and if we do not detect a photon in the first 30 readout cycles, we refer it as the $|\Downarrow\rangle$ state. After initialization check, we analyze the last 250 cycles. This conditional single-shot readout results are shown in Fig. 3(e). Finally, we achieve an average single-shot readout fidelity of $96.3 \pm 0.16\%$, which is limited by the false-negative probability $p(\Uparrow|\Downarrow) = 0.052$ and the false-positive probability $p(\Downarrow|\Uparrow) = 0.022$.

Furthermore, by sacrificing the readout success efficiency, we can achieve higher single-shot readout fidelity with the dual-step single-shot readout scheme [26], as depicted in Fig. 4(a). The initialization process is the same as above, and a single-shot readout process consists of N_2 readout cycles. During each readout cycle, we first apply

two CNOT gates (MW1A and MW3A π pulse) on the V2 electron spin and 1.5 µs $A2$ readout laser for the first read, then we apply another two CNOT gates (MW1B and MW3B π pulse) on the V2 electron spin and 1.5 µs $A2$ readout laser for the second read. The first readout step recognizes $|\Uparrow\rangle$ as bright, while the second step recognizes $|\Downarrow\rangle$ as bright. We isolate the first 20 readout cycles to exclude the infidelity from nuclear initialization. The thresholds are the same as before.

After the first 20 cycles, we take the last 80 cycles as the result, with $N_2 = 100$. We give the correlation results in Figs. 4(b) and 4(c), with the nuclear spin initialized to $|\Uparrow\rangle$ and $|\Downarrow\rangle$, respectively. For each readout step, if the number of photons detected is equal or above a threshold, we denote the result as bright. Otherwise, we denote it as dark. In we only consider the subspace that the state is detected in as bright merely once in the two steps, we can achieve single-shot readout fidelity of $97.16 \pm 0.1\%$ with a success efficiency of 86.1%. Furthermore, by reducing N_2 [Fig. 4(d)] and improving the threshold to 2 [Fig. 4(e)], we can achieve the dual-step readout fidelity of $99.03 \pm 0.13\%$ with 10.7% success efficiency within 0.28 ms. It is worth noting that, when changing N_2, we still isolate the first 20 readout cycles among the total N_2 readout cycles to exclude the nuclear spin initialization error.

Based on our single-shot readout scheme, decreasing the nuclear flip-flop probability and improving the collection efficiency will improve the readout fidelity. First, to decrease the V2 center-nuclear flip-flop possibility, 4H-SiC with isotope engineering is crucial [27], which has been used in previous works and exhibits excellent coherence properties with V2 center Hahn-echo coherence time reaching 1.3 ms [12]. By using this sample, ultranarrow V2 center ODMR linewidth around 100 kHz can be achieved. When this V2 center is coupled with a ^{29}Si nuclear spin, which is a little farther than NNN ^{29}Si, the splitting of V2 center energy levels is about 2 MHz [28]. Under this energy splitting, two narrow V2 center ODMR peaks can still be manipulated independently. Smaller splitting means less coupling between V2 center and nuclear spin, which can significantly reduce the possibility of the flip-flop process during each readout cycle, and as a result, the nuclear single-shot readout fidelity can be almost perfect.

Second, to improve the collection efficiency, we can couple the V2 center to nanostructures [29], which have been demonstrated by many works before. The overall collection efficiency can be highly enhanced by at least 5 times after coupling with nanostructures such as photonic crystal cavities [30] or microdisk cavities [17] and collected by taper fibers [31] or grating couplers [32]. As a result, we can predict that the single-shot readout fidelity will achieve 99.7%. By combining crystal isotope engineering and cavity enhancement together, nuclear single-shot readout with high speed and almost perfect fidelity is expected in the future.
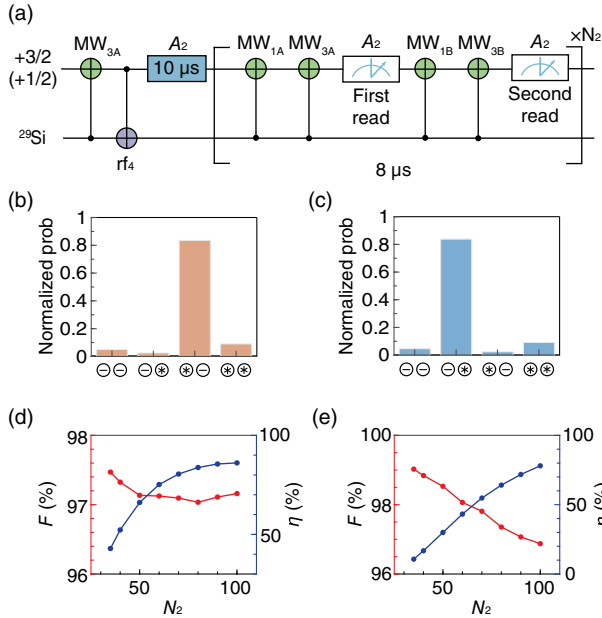

FIG. 4. Nuclear spin dual-step readout. (a) Circuit diagram of the scheme. (b),(c) Correlation results of the dual-step readout, with $N_2 = 100$ and threshold $= 1$. In (b), the nuclear spin is initialized to $|\Uparrow\rangle$, while in (c) the nuclear spin is initialized to $|\Downarrow\rangle$. For each step, a bright result is denoted as $\circledast$, and a dark result is denoted as $\ominus$. By considering the subspace of $\circledast\ominus$ and $\ominus\circledast$, the readout fidelity reaches $97.16 \pm 0.1\%$ with a success efficiency of 86.1%. (d),(e) Dependence of the readout fidelity and success efficiency on N_2. The threshold is set to 1 for (d) and to 2 for (e).

In conclusion, we perform the first demonstration of nuclear spin single-shot readout in silicon carbide by choosing an in plane ^{29}Si nuclear spin and applying a high magnetic field. The high readout fidelity demonstrated in this Letter creates opportunities for high fidelity nuclear photon entanglement with long lifetimes. Even though the optical pumping process includes complex dynamics in the V2 center, the nuclear flip-flop process is slow enough to perform single-shot readout by using the in plane NNN ^{29}Si nuclear spin. The coherence properties of V2 electron spins and nuclear spins can be improved by crystal engineering, such as isotope purification and decreasing of impurity concentration. Thanks to weak coupling to the stray electric field and strain, V2 center in silicon carbide can be integrated into nanophotonic structures, such as 1D photonic crystal and microdisk cavities. When the cavity is strongly coupled, the single-shot readout speed and fidelity will be greatly improved. The ZPL wavelength of the V2 centers can be converted to telecom U band with a pump laser near 2051 nm, allowing long-distance transmission in optical fibers [33]. With these improvements, the V2 center in SiC may become a highly competitive approach for quantum networks [34].

Note added.—Recently, we became aware of a related experiment with similar results [35].

---

*These authors contributed equally to this work.

[1] D. D. Awschalom, R. Hanson, J. Wrachtrup, and B. B. Zhou, Nat. Photonics **12**, 516 (2018).

[2] M. Ruf, N. H. Wan, H. Choi, D. Englund, and R. Hanson, J. Appl. Phys. **130**, 070901 (2021).

[3] M. Atatüre, D. Englund, N. Vamivakas, S.-Y. Lee, and J. Wrachtrup, Nat. Rev. Mater. **3**, 38 (2018).

[4] G. Wolfowicz, F. J. Heremans, C. P. Anderson, S. Kanai, H. Seo, A. Gali, G. Galli, and D. D. Awschalom, Nat. Rev. Mater. **6**, 906 (2021).

[5] N. T. Son, C. P. Anderson, A. Bourassa, K. C. Miao, C. Babin, M. Widmann, M. Niethammer, J. Ul Hassan, N. Morioka, I. G. Ivanov, F. Kaiser, J. Wrachtrup, and D. D. Awschalom, Appl. Phys. Lett. **116**, 190501 (2020).

[6] D. M. Lukin, M. A. Guidry, and J. Vučković, PRX Quantum **1**, 020102 (2020).

[7] D. M. Lukin, C. Dory, M. A. Guidry, K. Y. Yang, S. D. Mishra, R. Trivedi, M. Radulaski, S. Sun, D. Vercruysse, G. H. Ahn, and J. Vučković, Nat. Photonics **14**, 330 (2020).

[8] R. Nagy, M. Niethammer, M. Widmann, Y.-c. Chen, P. Udvarhelyi, C. Bonato, J. U. Hassan, R. Karhu, I. G. Ivanov, N. T. Son, J. R. Maze, T. Ohshima, Ö. O. Soykal, Á. Gali, S.-y. Lee, F. Kaiser, and J. Wrachtrup, Nat. Commun. **10**, 1954 (2019).

[9] H. B. Banks, Ö. O. Soykal, R. L. Myers-Ward, D. K. Gaskill, T. L. Reinecke, and S. G. Carter, Phys. Rev. Appl. **11**, 024013 (2019).

[10] A. Bourassa, C. P. Anderson, K. C. Miao, M. Onizhuk, H. Ma, A. L. Crook, H. Abe, J. Ul-Hassan, T. Ohshima, N. T. Son *et al.*, Nat. Mater. **19**, 1319 (2020).

[11] N. Morioka *et al.*, Nat. Commun. **11**, 2516 (2020).

[12] C. Babin *et al.*, Nat. Mater. **21**, 67 (2021).

[13] C. P. Anderson, E. O. Glen, C. Zeledon, A. Bourassa, Y. Jin, Y. Zhu, C. Vorwerk, A. L. Crook, H. Abe, J. Ul-Hassan, T. Ohshima, N. T. Son, G. Galli, and D. D. Awschalom, Sci. Adv. **8**, eabm5912 (2022).

[14] R.-Z. Fang, X.-Y. Lai, T. Li, R.-Z. Su, B.-W. Lu, C.-W. Yang, R.-Z. Liu, Y.-K. Qiao, C. Li, Z.-G. He *et al.*, arXiv:2311.17455.

[15] P. Udvarhelyi, G. Thiering, N. Morioka, C. Babin, F. Kaiser, D. Lukin, T. Ohshima, J. Ul-Hassan, N. T. Son, J. Vučković *et al.*, Phys. Rev. Appl. **13**, 054017 (2020).

[16] D. Liu, F. Kaiser, V. Bushmakin, E. Hesselmeier, T. Steidl, T. Ohshima, N. T. Son, J. Ul-Hassan, Ö. O. Soykal, and J. Wrachtrup, arXiv:2307.13648.

[17] D. M. Lukin, M. A. Guidry, J. Yang, M. Ghezellou, S. Deb Mishra, H. Abe, T. Ohshima, J. Ul-Hassan, and J. Vučković, Phys. Rev. X **13**, 011005 (2023).

[18] J. Heiler, J. Körber, E. Hesselmeier, P. Kuna, R. Stöhr, P. Fuchs, M. Ghezellou, J. Ul-Hassan, W. Knolle, C. Becher *et al.*, arXiv:2310.12617.

[19] O. Bulancea-Lindvall, M. T. Eiles, N. T. Son, I. A. Abrikosov, and V. Ivády, Phys. Rev. Appl. **19**, 064046 (2023).

[20] A. Reiserer, N. Kalb, M. S. Blok, K. J. M. van Bemmelen, T. H. Taminiau, R. Hanson, D. J. Twitchen, and M. Markham, Phys. Rev. X **6**, 021040 (2016).

[21] P.-J. Stas, Y. Q. Huan, B. Machielse, E. N. Knall, A. Suleymanzade, B. Pingault, M. Sutula, S. W. Ding, C. M. Knaut, D. R. Assumpcao *et al.*, Science **378**, 557 (2022).

[22] P. V. Klimov, A. L. Falk, D. J. Christle, V. V. Dobrovitski, and D. D. Awschalom, Sci. Adv. **1**, e1501015 (2015).

[23] A. L. Falk, P. V. Klimov, V. Ivády, K. Szász, D. J. Christle, W. F. Koehl, Á. Gali, and D. D. Awschalom, Phys. Rev. Lett. **114**, 247603 (2015).

[24] G. Waldherr, Y. Wang, S. Zaiser, M. Jamali, T. Schulte-Herbrüggen, H. Abe, T. Ohshima, J. Isoya, J. Du, P. Neumann *et al.*, Nature (London) **506**, 204 (2014).

[25] L. Jiang, J. Hodges, J. Maze, P. Maurer, J. Taylor, D. Cory, P. Hemmer, R. L. Walsworth, A. Yacoby, A. S. Zibrov *et al.*, Science **326**, 267 (2009).

[26] J. M. Kindem, A. Ruskuc, J. G. Bartholomew, J. Rochman, Y. Q. Huan, and A. Faraon, Nature (London) **580**, 201 (2020).

[27] I. G. Ivanov, M. Yazdanfar, B. Lundqvist, J.-T. Chen, J. Hassan, P. Stenberg, R. Liljedahl, N. T. Son, J. W. Ager, O. Kordina *et al.*, in *Materials Science Forum* (Trans Tech Publisher, Dürnten, 2014), Vol. 778, pp. 471–474.

[28] E. Hesselmeier, P. Kuna, I. Takács, V. Ivády, W. Knolle, N. T. Son, M. Ghezellou, J. Ul-Hassan, D. Dasari, F. Kaiser *et al.*, Phys. Rev. Lett. **132**, 090601 (2024).

[29] S. Majety, P. Saha, V. A. Norman, and M. Radulaski, J. Appl. Phys. **131**, 130901 (2022).

[30] D. M. Lukin, C. Dory, M. A. Guidry, K. Y. Yang, S. D. Mishra, R. Trivedi, M. Radulaski, S. Sun, D. Vercruysse, G. H. Ahn *et al.*, Nat. Photonics **14**, 330 (2020).

[31] C. T. Nguyen, D. D. Sukachev, M. K. Bhaskar, B. Machielse, D. S. Levonian, E. N. Knall, P. Stroganov, R. Riedinger, H. Park, M. Lončar, and M. D. Lukin, Phys. Rev. Lett. **123**, 183602 (2019).

[32] C. Dory, D. Vercruysse, K. Y. Yang, N. V. Sapra, A. E. Rugar, S. Sun, D. M. Lukin, A. Y. Piggott, J. L. Zhang, M. Radulaski *et al.*, Nat. Commun. **10**, 3309 (2019).

[33] Y. Yu, F. Ma, X. Y. Luo, B. Jing, and J. W. Pan, Nature (London) **578**, 240 (2020).

[34] S. Wehner, D. Elkouss, and R. Hanson, Science **362**, eaam9288 (2018).

[35] E. Hesselmeier, P. Kuna, W. Knolle, F. Kaiser, N. T. Son, M. Ghezellou, J. Ul-Hassan, V. Vorobyov, and J. Wrachtrup, following Letter, Phys. Rev. Lett. **132**, 180804 (2024).